Mechanical Systems and Signal Processing 24 (2010) 623–635

Contents lists available at ScienceDirect

Mechanical Systems and Signal Processing

journal homepage: www.elsevier.com/locate/jnlabr/ymssp

Structural health monitoring using shaped sensors

M.I. Friswell *, S. Adhikari

School of Engineering, Swansea University, Singleton Park, Swansea SA2 8PP, UK

ARTICLE INFO

Article history:
Received 10 June 2009
Received in revised form
10 September 2009
Accepted 15 October 2009
Available online 28 October 2009

Keywords:
SHM
Piezoelectric sensors
Shaped sensors
Selective sensitivity

ABSTRACT

This paper is concerned with distributed sensors to measure the response of beam and plate structures. The design of modal sensors for beam structures is well established. The design for plate structures with constant thickness sensors may be achieved by optimizing the shape of the sensor boundary, or by optimizing the effectiveness of the electrode. Most applications consider vibration control, but this paper is concerned with structural health monitoring, where the sensor output is made sensitive to changes in key stiffness parameters, for example in joints. The procedure is based on finite element models of the structures, and thus distributed transducers may be designed for arbitrary beam and plate structures. Simulated examples of a beam and a plate excited by a rotating machine are used to demonstrate the approach.

1. Introduction

The idea of using modal sensors and actuators for beam and plate type structures has been a subject of intense interest for many years. Using modal sensors in active control reduces problems of spillover, where high frequency unmodeled modes affect the stability of the closed loop system. The sensors and actuators may be discrete or distributed, and are usually manufactured using piezoelectric material, such as polyvinylidene fluoride (PVDF) film. For example, a modal sensor for a beam type structure may be obtained by varying the sensor width along the length of the beam. If the sensor covers the whole beam the shape of the sensor may be derived using the mode shape orthogonality property [1,2]. Modal sensors may be designed that cover only part of the beam [3], or are segmented sensors sensitive to multiple modes. The effect of geometric tolerances during manufacture on the quality of the sensors may be determined [3]. For beam structures the width of the sensor may be parameterized using the finite element method and the underlying shape functions used to approximate the transducer shape [4].

For two-dimensional structures, the approach used for beams may be implemented by varying the thickness of the PVDF, although this is very difficult to achieve in practice. Sun et al. [5] replaced an actuator layer with variable thickness by many small segments of uniform thickness. Kim et al. [6,7] developed two design methods for distributed modal transducers for composite plates, the first using multi-layered PVDF films with optimized electrode pattern, lamination angle, and poling direction, and the second using PVDF film segments and an interface circuit. Preumont et al. [8] introduced the porous electrode concept, which allows the gains to be introduced by changing the local effectiveness of the electrodes. The alternative is to design a distributed modal transducer by optimizing the continuous boundary shape of a constant thickness PVDF film by assuming a smooth boundary [9–11] or using topology optimization methods [12–14].

* Corresponding author.
E-mail addresses: m.i.friswell@swansea.ac.uk (M.I. Friswell), s.adhikari@swansea.ac.uk (S. Adhikari).
URLS: http://michael.friswell.com (M.I. Friswell), http://engweb.swan.ac.uk/~adhikaris (S. Adhikari).

0888-3270/$ - see front matter © 2009 Elsevier Ltd. All rights reserved.
doi:10.1016/j.ymssp.2009.10.009

This paper uses the design methods for modal sensors, but extends this approach to the structural health monitoring application.

The identification of the location and severity of cracks, loose bolts and other types of damage in structures using vibration data has received considerable attention [15]. Most of the approaches use the modal data of a structure before damage occurs as baseline data, and all subsequent tests are compared to it [16–19]. Any deviation in the modal properties from this baseline data is used to estimate model parameters related to the damage severity and location. The advantage of using this baseline data is that some allowance is made for modeling errors. However changes in the structure not due to damage, for example due to environmental effects, will be difficult to distinguish from changes due to damage [20,21]. The approach adopted in this paper is to use shaped transducers to reduce the sensitivity of the sensor output to the unmodeled parameter changes and environmental effects. For structural health monitoring this means that the response can be made sensitive to particular regions of interest, so that, for example, the sensor may be used to monitor the health of a single joint. This concept is different to the usual approach in health monitoring where the key objective is to determine the location of damage. The assumption here is that we know of several regions that need to be monitored (for example, joints) and the motivation is to design a sensor that requires very little post processing to estimate the condition of the monitored region. Thus one sensor monitors one region of the structure, and multiple sensors could be used to monitor multiple regions. The method is an extension of the selective sensitivity technique which was developed to design excitations that produce strong sensitivities to a subset of the parameters whilst causing the sensitivities to other parameters to vanish. This concept is modified to choose the shaped sensor, although the spatial and spectral properties of the expected in-service excitation are still an important aspect of the design.

The finite element model of the structure is of the form

$$\mathbf{M}\ddot{\mathbf{q}} + \mathbf{D}\dot{\mathbf{q}} + \mathbf{K}\mathbf{q} = \mathbf{B}\mathbf{u}, \quad \mathbf{y} = \mathbf{C}\mathbf{q} \tag{1}$$

where **M**, **D** and **K** are the mass, damping and stiffness matrices based on the degrees of freedom, **q**. The inputs to the structure, **u**, are applied via a matrix, **B**, which determines the location and gain of the actuators (or the actuator shape for distributed actuators). Similarly the outputs, **y**, are obtained via the output matrix **C** which is determined by the sensor shape. For parameter estimation and health monitoring applications the mass, damping and stiffness matrices depend on a set of physical parameters, θ.

2. Defining shaped sensors

For beam structures whose response is predominantly in bending in a single plane, the transducer may be shaped by varying the width of the PVDF material. For beam and plate structures either the thickness [5–7] or the electrode effectiveness [8] (which may be considered equivalent to thickness) may be changed. In all these cases the width or thickness is assumed to be a continuous function. However this function needs to be parameterized to enable the optimization of the sensor. Using the shape functions of the underlying finite element model is a convenient approach to approximate the width or thickness of the piezoelectric material [4]. In this way modal transducers may be designed for arbitrary beam or plate type structures, and the sensor width or thickness (and often its slope also) will be continuous across the element boundaries. Furthermore modal transducers that only cover part of a structure may be designed. Most of the development will concern sensors, although actuators may be dealt with in a similar way.

The approach is developed using simple models of the structure and assuming an isotropic piezoelectric material, although the concept could be extended to a general piezoelectric formulation. The integration within a commercial finite element code is outside the scope of this paper, and would require the calculation and assembly of extra element matrices.

For a plate element, the output (voltage or charge) from the part of the sensor covering element number e is [5]

$$y_e(t) = K_s \iint f_e(\xi,\eta)\left(\frac{\partial^2 w_e(\xi,\eta,t)}{\partial \xi^2} + \frac{\partial^2 w_e(\xi,\eta,t)}{\partial \eta^2}\right) \mathrm{d}\xi\, \mathrm{d}\eta \tag{2}$$

where $f_e(\xi,\eta)$ defines the effectiveness of the sensor at location (ξ,η) which incorporates the sensor thickness (or possibly distance from the plate neutral plane), the piezoelectric coefficient and also the polarization direction. Here a Cartesian coordinate system is used and the integration is performed over the element, although other coordinate systems could be used. w_e is the plate deflection within the element. K_s is a constant relating to the piezoelectric properties. For a rectangular plate element, with dimensions $2a$ and $2b$ in the ξ and η directions respectively, the output would be

$$y_e(t) = K_s \int_{-b}^{b}\int_{-a}^{a} f_e(\xi,\eta)\left(\frac{\partial^2 w_e(\xi,\eta,t)}{\partial \xi^2} + \frac{\partial^2 w_e(\xi,\eta,t)}{\partial \eta^2}\right) \mathrm{d}\xi\, \mathrm{d}\eta \tag{3}$$

For a beam element of length ℓ_e the output is

$$y_e(t) = K_s \int_0^{\ell_e} f_e(\xi)\frac{\partial^2 w_e(\xi,t)}{\partial \xi^2}\, \mathrm{d}\xi \tag{4}$$

where now the sensor effectiveness $f_e(\xi)$ allows for varying width, as well as (possibly) varying electrode effectiveness or thickness. The development will concentrate on sensors for plate structures, although it is clear that the results for beam

structures will be a special case. Sensor thickness will be used, although this should be interpreted as sensor effectiveness for plates, and sensor width for beams.

The objective is to approximate the continuous sensor effectiveness using a discrete set of parameters, based on the finite element shape functions. In finite element analysis the displacement is approximated as

$$w_e(\xi,\eta) = \mathbf{N}(\xi,\eta)\mathbf{q}_e \tag{5}$$

where $\mathbf{N}(\xi,\eta)$ are the shape functions and $\mathbf{q}_e$ are the nodal generalized displacements. Suppose that the sensor thickness is also approximated by the shape functions, so that

$$f_e(\xi,\eta) = \mathbf{N}(\xi,\eta)\mathbf{f}_{se} \tag{6}$$

where $\mathbf{f}_{se}$ is a vector of the same length as the nodal displacements, that defines the thickness of the sensor. In this way the continuous sensor thickness is approximated using a finite set of parameters in $\mathbf{f}_{se}$. Substituting into Eq. (2) gives

$$y_e(t) = \mathbf{f}_{se}^{\top}\mathbf{C}_{se}\mathbf{q}_e \tag{7}$$

where

$$\mathbf{C}_{se} = K_s \iint \mathbf{N}(\xi,\eta)^{\top}\left(\frac{\partial^2\mathbf{N}(\xi,\eta)}{\partial\xi^2} + \frac{\partial^2\mathbf{N}(\xi,\eta)}{\partial\eta^2}\right)\mathrm{d}\xi\,\mathrm{d}\eta \tag{8}$$

If a commercial finite element code were employed then the matrix $\mathbf{C}_{se}$ would have to be computed for the elements used.

The total sensor output is obtained by summing the output from all of the elements. Thus

$$y = \sum_e y_e = \mathbf{f}_s^{\top}\mathbf{C}_s\mathbf{q} \tag{9}$$

where $\mathbf{q}$ is the vector of generalized displacements of the full model, and $\mathbf{f}_s$ is a vector incorporating the sensor parameter vectors. In this way, the problem of a continuous thickness variation is changed into a discrete optimization problem for $\mathbf{f}_s$. The assembly process is exactly analogous to the assembly of mass and stiffness matrices in standard finite element analysis. The only slight difference is the incorporation of boundary conditions. For example a pinned boundary will require that some of the generalized displacements are set to zero, which reduces the number of degrees of freedom. Just because a generalized displacement at a given node is zero does not mean that the corresponding element of the sensor thickness parameters, $\mathbf{f}_s$, should be zero, as the sensor thickness may be non-zero at the boundary. In turn this means that $\mathbf{C}_s$ may be a rectangular matrix. Comparing Eqs. (1) and (9) it is clear that $\mathbf{C} = \mathbf{f}_s^{\mathrm{T}}\mathbf{C}_s$.

For a beam element with cubic shape functions [4],

$$\mathbf{C}_{se} = -\frac{K_s}{30\ell_e}\begin{bmatrix} 36 & 33\ell_e & -36 & 3\ell_e \\ 3\ell_e & 4\ell_e^2 & -3\ell_e & -\ell_e^2 \\ -36 & -3\ell_e & 36 & -33\ell_e \\ 3\ell_e & -\ell_e^2 & -3\ell_e & 4\ell_e^2 \end{bmatrix} \tag{10}$$

For plate elements the matrices are relatively easy to generate, although difficult to express in a closed and compact form. Dawe [22] described the R1 rectangular element which has four nodes and three degrees of freedom per node. As an example, consider a square element with side $2a$. Then the element output matrix, $\mathbf{C}_{se}$, is

$$\frac{K_s}{720}\begin{bmatrix} -600 & -120a & -120a & 168 & 48a & 0 & 264 & -72a & -72a & 168 & 0 & 48a \\ -552a & -143a^2 & -159a^2 & -240a & -79a^2 & 111a^2 & 24a & 31a^2 & 15a^2 & 48a & 47a^2 & -15a^2 \\ -552a & -159a^2 & -143a^2 & 48a & -15a^2 & 47a^2 & 24a & 15a^2 & 31a^2 & -240a & 111a^2 & -79a^2 \\ 168 & 48a & 0 & -600 & -120a & 120a & 168 & 0 & -48a & 264 & -72a & 72a \\ -240a & -79a^2 & -111a^2 & -552a & -143a^2 & 159a^2 & 48a & 47a^2 & 15a^2 & 24a & 31a^2 & -15a^2 \\ -48a & 15a^2 & 47a^2 & 552a & 159a^2 & -143a^2 & 240a & -111a^2 & -79a^2 & -24a & -15a^2 & 31a^2 \\ 264 & 72a & 72a & 168 & 0 & -48a & -600 & 120a & 120a & 168 & -48a & 0 \\ -24a & 31a^2 & 15a^2 & -48a & 47a^2 & -15a^2 & 552a & -143a^2 & -159a^2 & 240a & -79a^2 & 111a^2 \\ -24a & 15a^2 & 31a^2 & 240a & 111a^2 & -79a^2 & 552a & -159a^2 & -143a^2 & -48a & -15a^2 & 47a^2 \\ 168 & 0 & 48a & 264 & 72a & -72a & 168 & -48a & 0 & -600 & 120a & -120a \\ -48a & 47a^2 & 15a^2 & -24a & 31a^2 & -15a^2 & 240a & -79a^2 & -111a^2 & 552a & -143a^2 & 159a^2 \\ -240a & -111a^2 & -79a^2 & 24a & -15a^2 & 31a^2 & 48a & 15a^2 & 47a^2 & -552a & 159a^2 & -143a^2 \end{bmatrix} \tag{11}$$

3. Health monitoring and selective sensitivity

A significant problem with any inverse problem, such as structural health monitoring, is ill-conditioning of the estimation equations. One major cause of this ill-conditioning is the large number of candidate parameters that may be

regarded as uncertain. Applying excitations that produce strong sensitivities to a subset of the parameters whilst causing the sensitivities to other parameters to vanish is one way of reducing the number of parameters to estimate. For structural health monitoring this means that the response can be made sensitive to particular regions of interest, so that, for example, the sensor may be used to monitor the health of a single joint. One approach to local structural health monitoring is to use high frequency impedance measurements [23], although using shaped distributed actuators and sensors could also be applied to these impedance techniques. Discrete spatial filters have been used for health monitoring using the vibration response [24–27] and for ultrasonic waves [28,29].

The method of selective sensitivity considers the response predictions to a relatively large number of excitation forces. In order to provide further explanation, the work of Ben-Haim [30–33] will be adapted to sensors rather than actuators. The selective sensitivity approach is best derived in the frequency domain. From Eq. (1):

$$\mathbf{y}(\omega,\theta)=\mathbf{C}[-\omega^2\mathbf{M}+\mathrm{j}\omega\mathbf{D}+\mathbf{K}]^{-1}\mathbf{B}\mathbf{u}(\omega)=\mathbf{f}^{\top}\mathbf{C}_s\mathbf{H}(\omega,\theta)\mathbf{B}\mathbf{u}(\omega) \tag{12}$$

where $\mathbf{H}(\omega,\theta)=[-\omega^2\mathbf{M}+\mathrm{j}\omega\mathbf{D}+\mathbf{K}]^{-1}$ is the frequency response function (receptance matrix).

At any frequency the sensitivity of the response to parameter θ_j is given by

$$S_j(\mathbf{f},\omega)=\left\|\frac{\partial y}{\partial\theta_j}\right\|^2 \tag{13}$$

Notice that only a single output has been assumed, so that y is a scalar, although the approach is easily extended to multiple outputs. Then

$$S_j(\mathbf{f},\omega)=\mathbf{f}^{\top}\mathbf{C}_s\frac{\partial\mathbf{H}}{\partial\theta_j}\mathbf{B}\mathbf{u}\mathbf{u}^{\mathrm{H}}\mathbf{B}^{\mathrm{H}}\frac{\partial\mathbf{H}^{\mathrm{H}}}{\partial\theta_j}\mathbf{C}_s^{\top}\mathbf{f}=\mathbf{f}^{\top}\mathbf{G}_j(\omega)\mathbf{f} \tag{14}$$

where $\mathbf{G}_j(\omega)$ may be calculated and the superscript H denotes the conjugate transpose. $\mathbf{G}_j(\omega)$ is usually complex, although it will be Hermitian from the definition in Eq. (14). Hence the real part of $\mathbf{G}_j(\omega)$ is symmetric and the imaginary part is skew-symmetric. Since $\mathbf{f}$ is real, the imaginary part of $\mathbf{G}_j(\omega)$ does not affect the sensitivity and may be neglected, and the sensitivity is real. Note that for excitation at a single location, $\mathbf{G}_j(\omega)$ has rank 1. The derivative of $\mathbf{H}$ may be calculated as

$$\frac{\partial\mathbf{H}}{\partial\theta_j}=-\mathbf{H}\left[-\omega^2\frac{\partial\mathbf{M}}{\partial\theta_j}+\mathrm{j}\omega\frac{\partial\mathbf{D}}{\partial\theta_j}+\frac{\partial\mathbf{K}}{\partial\theta_j}\right]\mathbf{H} \tag{15}$$

The sensitivity defined in Eq. (14) varies with frequency. For the standard selective sensitivity method the force input is designed and so may be varied with both location and frequency. With a shaped sensor for health monitoring the excitation is likely to be due to either ambient forces or operational conditions. Furthermore, to use a simple threshold to determine damage the output required is a single response quantity. In these cases an integrated sensitivity may be defined as

$$\hat{S}_j(\mathbf{f})=\int_{\omega_1}^{\omega_2}W(\omega)S_j(\mathbf{f},\omega)\,\mathrm{d}\omega \tag{16}$$

or some frequency weighting function $W(\omega)$ (that can be designed along with the sensor shape) and frequency range (ω_1,ω_2). For a given force input

$$\hat{S}_j(\mathbf{f})=\mathbf{f}^{\top}\left[\int_{\omega_1}^{\omega_2}W(\omega)\mathbf{G}_j(\mathbf{f},\omega)\mathrm{d}\omega\right]\mathbf{f}=\mathbf{f}^{\top}\hat{\mathbf{G}}_j\mathbf{f} \tag{17}$$

The design of suitable frequency weighting functions for particular applications is the subject of further investigation.

If the location and spectrum of the force is not known then this makes the design of a selectively sensitive sensor extremely difficult. If the location of the excitation were uncertain, then one possibility is to include a number of independent potential excitation locations. However this would increase the number of columns in $\mathbf{B}$, which would increase the rank of $\mathbf{G}_j$, and therefore reduce the chances of designing a suitable shaped sensor. Excitation at a single known location will be assumed in this paper. The rest of the development will consider only a single frequency using $\mathbf{G}_j(\omega)$ defined in Eq. (14), although the methods are readily extended to the frequency weighted versions using $\hat{\mathbf{G}}_j$ defined in Eq. (17).

The selective sensitivity problem for parameter s is to design the sensor such that

$$S_j(\mathbf{f})=\begin{cases}\neq 0 & \text{if } j=s\\ =0 & \text{otherwise}\end{cases} \tag{18}$$

Since the sensitivities are all real and non-negative, the conditions in Eq. (18) may be written as

$$S_s(\mathbf{f})=\mathbf{f}^{\top}\mathbf{G}_s\mathbf{f}\neq 0,\quad \sum_{j\neq s}S_j(\mathbf{f})=\sum_{j\neq s}\mathbf{f}^{\top}\mathbf{G}_j\mathbf{f}=\mathbf{f}^{\top}\tilde{\mathbf{G}}_s\mathbf{f}=0 \tag{19}$$

where $\tilde{\mathbf{G}}_s=\sum_{j\neq s}\mathbf{G}_j$.

Solving the selective sensitivity requirements exactly is often not possible, in the sense that a solution may not exist, or may not be unique. One straight-forward approach is to employ an optimization scheme directly. For example the sensor

shape $\mathbf{f}$ sensitive to parameter θ_s is obtained as the vector that minimizes the objective function

$$J(\mathbf{f}) = \left\{ \sum_{j \neq s} W_j S_j(\mathbf{f}) \right\} / S_s(\mathbf{f}) \tag{20}$$

where W_j are weighting factors for the different parameters. The thickness of the sensor is then normalized to the maximum thickness required.

3.1. Designing the sensor shape

The simple approaches to calculate the sensor shape may lead to difficulties if the solution is not unique and hence there are many solutions for perfect sensors that satisfy Eq. (18). If the excitation is at a single degree of freedom then the complex matrix $\mathbf{G}_j(\omega)$ will have rank 1, although the real part alone will usually have rank 2. If there are p parameters, and the response should be insensitive to $p-1$ of them, then the dimension of the space of suitable sensor shape vectors, $\mathbf{f}$, based on Eq. (18), is $n-2p+2$, where n is the length of the vector $\mathbf{f}$. In this case one has to introduce other regularizing conditions into the optimization. One possibility is to reduce the number of elements that the sensor covers, and subset selection techniques could be used to determine the optimum choice of elements. Another possibility is to minimize the transducer curvature [4], which has the advantage of producing sensors that are easier to manufacture. For beam structures, minimizing transducer curvature for a sensor covering the whole beam was shown to be equivalent to minimizing $\mathbf{f}^\top \hat{\mathbf{K}} \mathbf{f}$ where $\hat{\mathbf{K}}$ is the stiffness matrix for the free–free beam. This is equivalent to minimizing a strain energy type expression, and motivates the optimization problem for the general system.

The best approach is to enforce the zero sensitivity to unwanted parameters before optimizing any other objectives. Thus a transformation, $\mathbf{T}$, is introduced such that

$$\mathbf{T}^\top \tilde{\mathbf{G}}_s \mathbf{T} = \mathbf{0} \tag{21}$$

This transformation matrix may be found easily using the singular value decomposition of $\tilde{\mathbf{G}}_s$ (which is equivalent to the eigenvalue problem since the real part of $\tilde{\mathbf{G}}_s$ is symmetric), and will generally be of dimension $n \times (n-2p+2)$. Thus a reduced dimension sensor vector $\mathbf{f}_r$ may be defined such that $\mathbf{f} = \mathbf{T}\mathbf{f}_r$, and is chosen by minimizing

$$J(\mathbf{f}) = \mathbf{f}_r^\top [\mathbf{T}^\top \hat{\mathbf{K}} \mathbf{T}] \mathbf{f}_r \tag{22}$$

subject to

$$S_s(\mathbf{f}) = \mathbf{f}^\top \mathbf{G}_s \mathbf{f} = \mathbf{f}_r^\top [\mathbf{T}^\top \mathbf{G}_s \mathbf{T}] \mathbf{f}_r \neq 0 \tag{23}$$

This is easily solved by calculating the eigenvalues of $\mathbf{T}^\top \tilde{\mathbf{K}} \mathbf{T}$, and taking the eigenvector corresponding to the smallest eigenvalue, consistent with Eq. (23). An alternative is to maximize the sensitivity $S_s(\mathbf{f})$ by choosing $\mathbf{f}_r$ as the eigenvector corresponding to the largest eigenvalue of $\mathbf{T}^\top \mathbf{G}_s \mathbf{T}$.

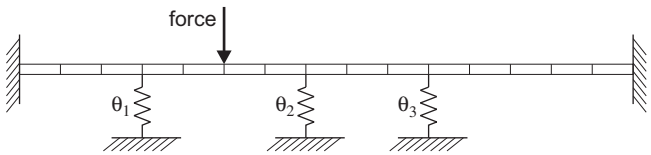

Fig. 1. The beam with intermediate supports and harmonic excitation.

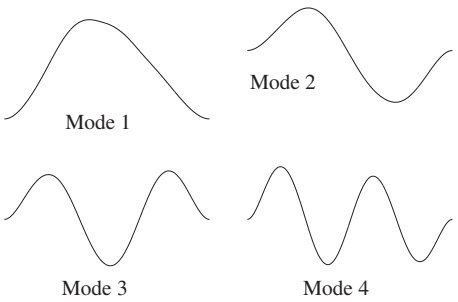

Fig. 2. The first four mode shapes of the beam with intermediate supports.

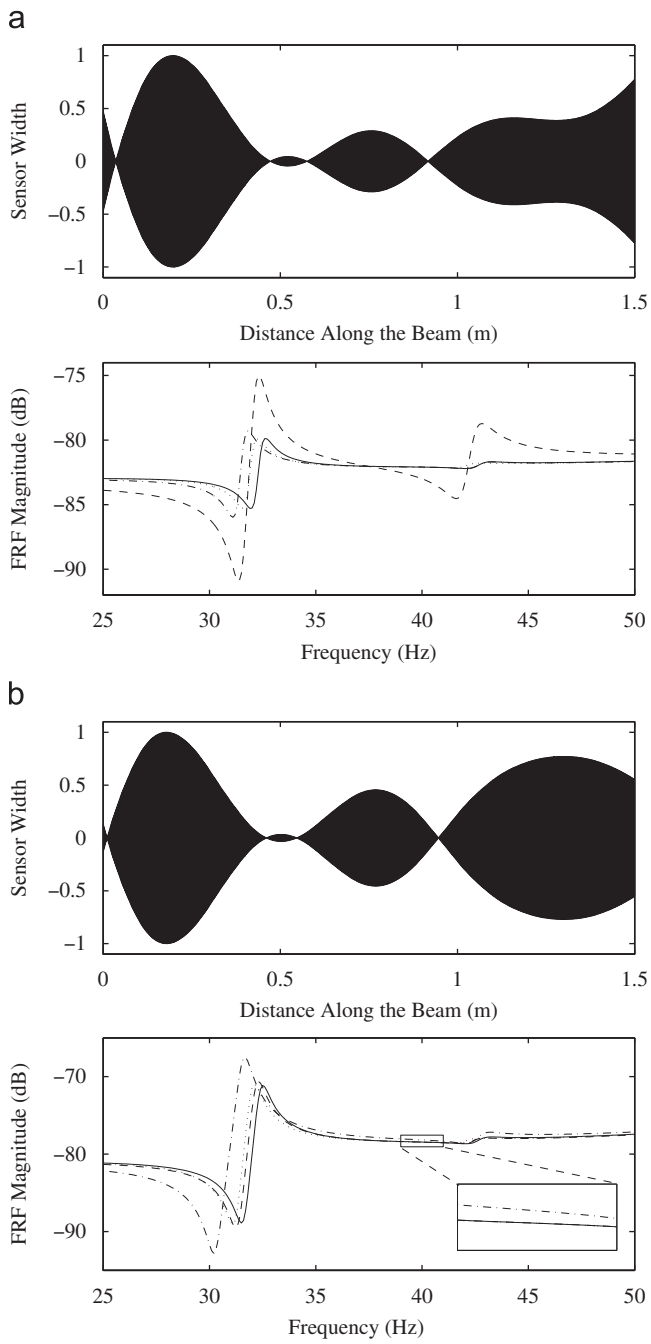

Fig. 3. The distributed sensor shape designed to be sensitive to particular support stiffnesses at 40 Hz for the beam example, and the associated receptances. The solid line is the baseline FRF, the dashed line is due to a 10% change in support stiffness 1, the dot-dashed line is due to a change in stiffness 2, and the dotted line is due to a change in stiffness 3: (a) sensitive to support 1 and (b) sensitive to support 2 (note the zoomed FRF in the range 39–41 Hz).

4. A simulated beam example

A clamped–clamped beam example inspired by Gawronski [34] will be used here to demonstrate the feasibility of the approach. The steel beam is 1.5 m long with cross-section 20×5 mm, and bending in the more flexible plane is modeled using 15 finite elements. The beam has three further supports along its length, modeled as springs at nodes 4, 8 and 11, where the node numbering convention means that node 1 is clamped, see Fig. 1. The nominal spring stiffnesses of the supports are 10 kN/m. The first four natural frequencies of the system are 32.4, 42.7, 70.1 and 109.0 Hz and the corresponding modes are shown in Fig. 2. For comparison, the corresponding natural frequencies for the beam without

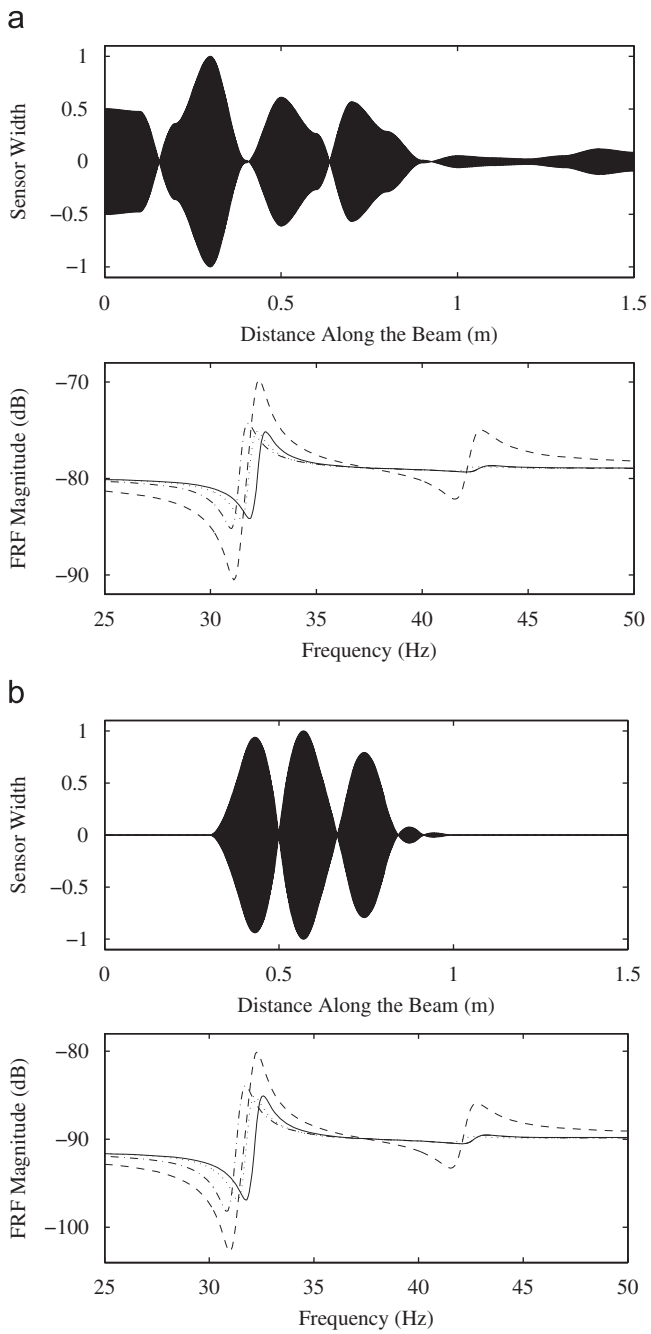

Fig. 4. The distributed sensor shape designed to be sensitive to support stiffness 1 at 40 Hz for the beam example, and the associated receptances. The solid line is the baseline FRF, the dashed line is due to a 10% change in support stiffness 1, the dot-dashed line is due to a change in stiffness 2, and the dotted line is due to a change in stiffness 3: (a) maximize sensitivity to support 1 and (b) restrict sensor region.

spring supports are 11.8, 32.6, 63.9 and 105.6 Hz. The damping is assumed to be proportional to stiffness with a factor of 10^{-4} s. The force is applied from a rotating machine operating at 40 Hz at node 6. The distributed sensor is to be designed for the whole length of the beam initially. The parameters of interest are the three support stiffnesses.

Fig. 3(a) shows the sensor shape obtained by minimizing the objective function in Eq. (22) for the first support stiffness. Note that $\mathbf{T}^{\top}\tilde{\mathbf{K}}\mathbf{T}$ has two zero eigenvalues that produce zero sensitivity to the first parameter and are therefore not chosen. The sensor width is normalized so that the maximum width is 1. The result is sensitivity ratios of $S_1/S_2 = 1.2 \times 10^{15}$ and $S_1/S_3 = 8.7 \times 10^{12}$, demonstrating that the required sensitivity is obtained. Also shown is the frequency response between the force input location and the sensor output. The baseline (solid line) is based on the undamaged system, and the responses due to a 10% reduction in each of the three support stiffnesses in turn are also shown. Remember that the sensor

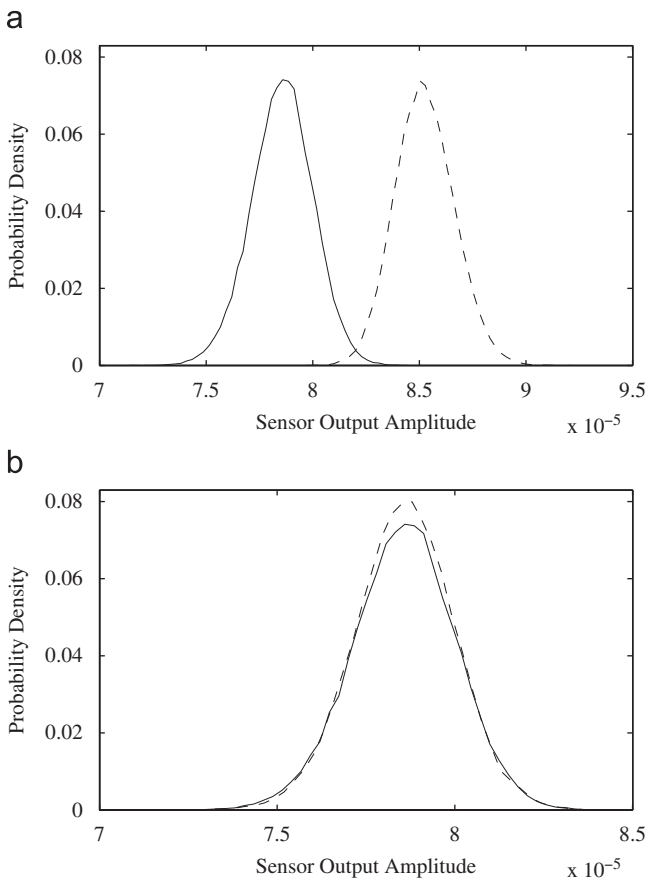

Fig. 5. The probability density function of the output from the distributed sensor in Fig. 2(a) to uncertainties in the support stiffnesses with 2% standard deviation. The solid line is for the nominal value of the stiffnesses and the dashed line due to the parameter increase: (a) 10% increase in θ_1 and (b) 10% increase in θ_2.

has been designed to operate only at 40 Hz, and at this frequency the response is indeed insensitive to changes in support stiffnesses 2 and 3. Fig. 3(b) shows the equivalent plots when the sensor is designed to be sensitive to support stiffness 2, also at 40 Hz. Although the FRF at 40 Hz is not sensitive to parameter 1 or 3, as demonstrated by the zoomed plot area in the figure, the sensitivity to parameter 2 is not very high. It is clear that the procedure has designed sensors with relatively simple shapes in both cases.

Suppose now that the sensor shape is chosen to maximize the sensitivity to the first parameter. The result is shown in Fig. 4(a), and highlights that the sensor shape is now more complicated. The sensitivity to parameter 1 is now over 600 times higher than that for the sensor in Fig. 3(a). Fig. 4(b) shows the effect of restricting the region where the sensor is placed, by setting the elements of the parameter vector $\mathbf{f}$ corresponding to finite element nodes 1–4 and 11–16 to zero. The sensor is designed to ensure zero sensitivity to parameters 2 and 3 and the minimum curvature solution is chosen. There is clearly a compromise between the smaller region for the sensor and the complexity of the shape.

The examples thus far have considered the design of the sensors and have shown the frequency response function over a large frequency range. We now consider the performance of the sensor when there is noise and errors in the system. The three stiffness parameters are assumed to be uncertain with a Gaussian distribution with a 2% standard deviation based on the nominal values of the stiffness. Fig. 5(a) shows the probability density function of the output of the sensor at 40 Hz due to these uncertainties at the nominal values of stiffness (solid) and when the value of the first stiffness changes by 10%. Clearly the output is able to distinguish that the first support has changed significantly. The probability density was calculated using a Monte Carlo simulation with 10,000 samples. Fig. 5(b) shows the equivalent result for a 10% change to the second stiffness parameter and shows that the sensor is insensitive to large changes in this stiffness.

Suppose now that the stiffness of the *clamped* supports also varies, perhaps due to environmental factors. This is modeled by varying the stiffness of the elements nearest to the clamped ends. Fig. 6 shows the sensor shape that is sensitive to support stiffness 1, and insensitive to support stiffnesses 2 and 3, and also the stiffnesses of the elements nearest the clamped ends. Also shown are the FRFs for the nominal values of the parameters, and for 10% reductions in all of the parameters. Interestingly the FRF is relatively insensitive to the element stiffnesses over the whole frequency range, although only the response at 40 Hz is used in the design. The environment will also change global parameters, such as the

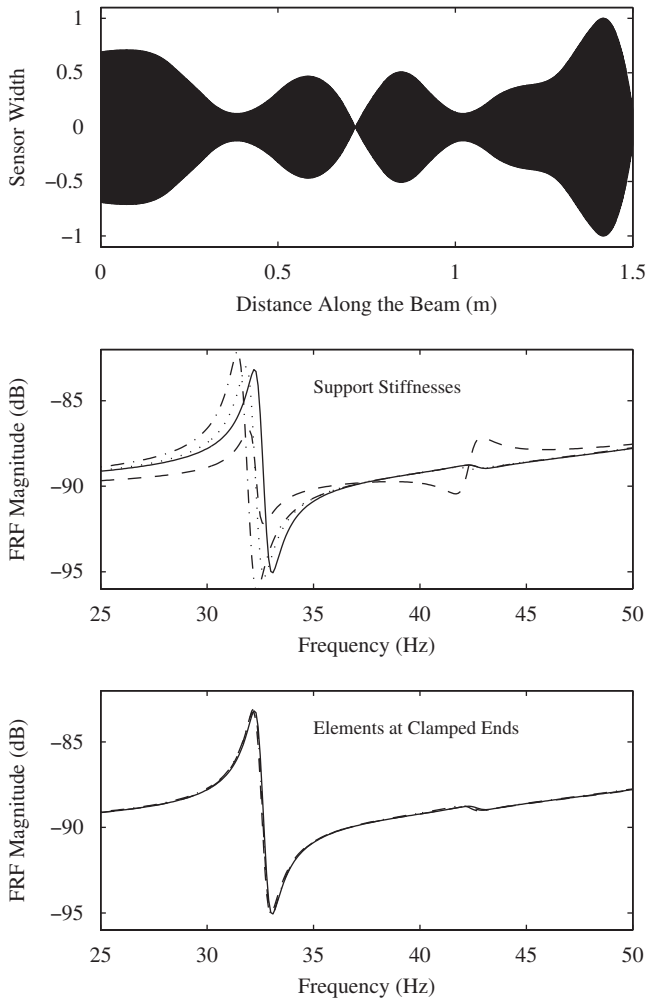

Fig. 6. The distributed sensor shape designed to be sensitive to support stiffness 1 at 40 Hz for the beam example and insensitive to the clamp stiffnesses, and the associated receptances. The solid line is the baseline FRF, and the other FRFs represent 10% changes to the support stiffnesses (dashed for support 1, dot-dashed for support 2, dotted for support 3) or the stiffness of the elements near the clamped ends (dashed for the left end, dot-dashed for the right end).

Young's modulus of the whole beam. Suppose a sensor is designed to be insensitive to support stiffnesses 2 and 3, and also to the global flexural rigidity of the beam. The result is shown in Fig. 7 and demonstrates that shaped sensors can be designed to be insensitive to global parameters.

The examples thus far have considered excitation at a single frequency, namely 40 Hz. Suppose now we consider excitation at 30, 35 and 40 Hz, and we set the frequency weighting to unity. The objective is to make the response sensitive to support stiffness 1 and insensitive to support stiffnesses 2 and 3. The output of the sensor for the nominal support stiffnesses, shown in Fig. 8, is approximately constant across the frequency range. Clearly the objective has been met and the response is only sensitive to support stiffness 1. Note that the sensor shape is now only slightly more complex than that in Fig. 3(b), despite the increase in the number of frequencies considered from one to three.

5. A simulated plate example

Consider now a rectangular steel plate of dimensions 400×300 mm and of thickness 7 mm. The plate is supported at each of its corners by a spring of stiffness 500 kN/m. The finite element model has 16×12 elements, so that each element is 25 mm square, as shown in Fig. 9. The first four natural frequencies of the system are 21.0, 44.7, 48.8 and 72.7 Hz and the corresponding modes are shown in Fig. 10. The damping is assumed to be proportional to stiffness with a factor of 10^{-4} s. The force is applied from a rotating machine operating at 40 Hz at the node shown in Fig. 9 by a circle. The distributed sensor is to be designed for the whole plate.

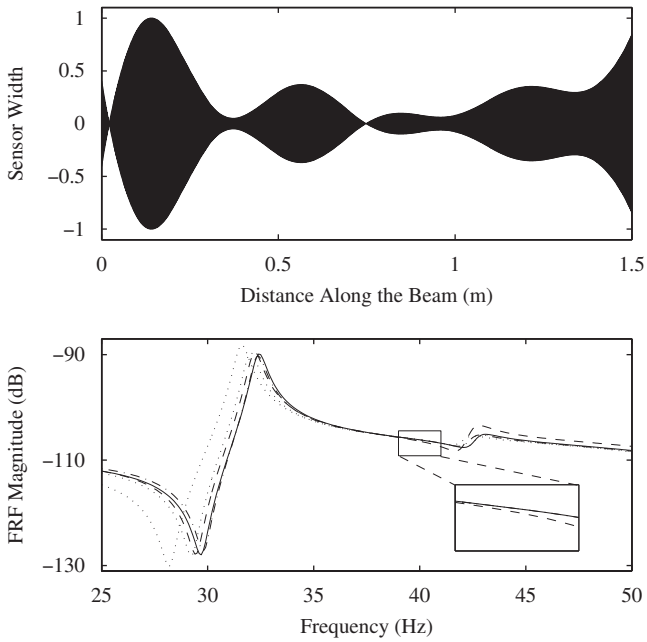

Fig. 7. The distributed sensor shape designed to be sensitive to support stiffness 1 at 40 Hz for the beam example and insensitive to the beam flexural rigidity, and the associated receptances. The solid line is the baseline FRF, the dashed line is due to a 10% change in support stiffness 1, the dotted lines are due to change in support stiffnesses 2 and 3, and the dot-dashed line is due to a 2% change in the flexural rigidity of the beam. Note the zoomed plot in the frequency range 39–41 Hz.

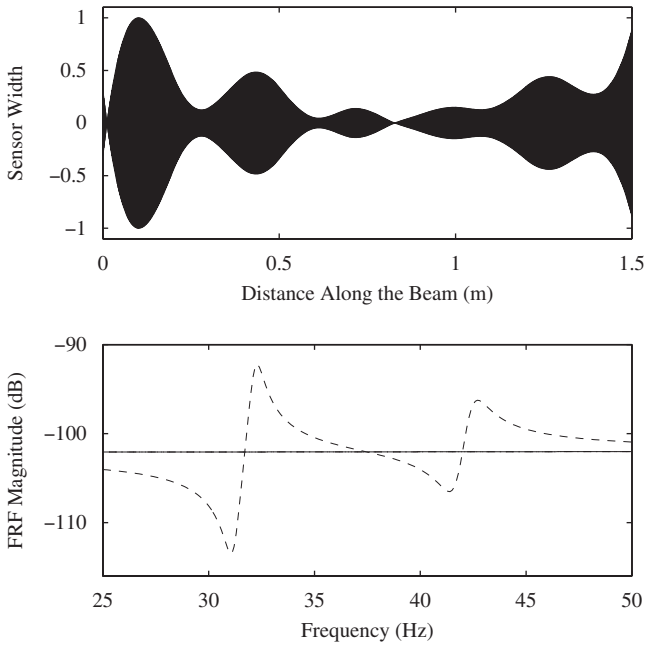

Fig. 8. The distributed sensor shape designed to be sensitive to support stiffness 1 at 30, 35 and 40 Hz for the beam example, and the associated receptances. The solid line is the baseline FRF, the dashed line is due to a 10% change in support stiffness 1, the dot-dashed line is due to a change in stiffness 2, and the dotted line is due to a change in stiffness 3.

Fig. 11(a) shows the sensor shape sensitive to the first support stiffness, θ_1, only and insensitive to the other supports, obtained by minimizing the objective function in Eq. (22). Note that $\mathbf{T}^{\top}\tilde{\mathbf{K}}\mathbf{T}$ has three zero eigenvalues that produce zero sensitivity to the first parameter and are therefore not chosen. The sensor width is normalized so that the maximum thickness is 1. The result is sensitivity ratios of $S_1/S_2 = 7.0 \times 10^{14}$, $S_1/S_3 = 5.6 \times 10^{13}$ and $S_1/S_4 = 1.4 \times 10^{12}$, demonstrating that the required sensitivity is obtained. Fig. 11(b) shows the sensor shape designed to be sensitive only to the second support stiffness, θ_2, and the corresponding sensitivity ratios are $S_2/S_1 = 1.7 \times 10^9$, $S_2/S_3 = 6.3 \times 10^{11}$ and

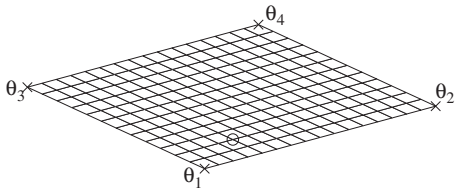

Fig. 9. The layout of the plate with corner support springs. The crosses denote the springs and the circle denotes the forcing position.

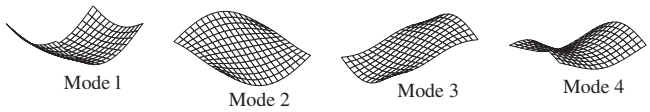

Fig. 10. The first four modes of the plate with corner supports.

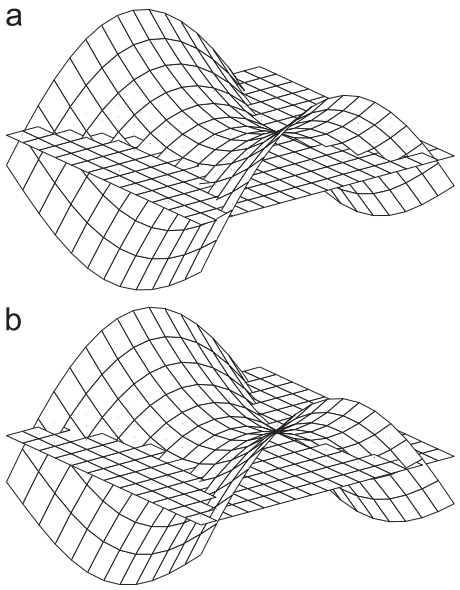

Fig. 11. The distributed sensor shape designed to be sensitive to the support stiffnesses at 40 Hz for the plate example, obtained by minimizing curvature: (a) maximize sensitivity to support 1 and (b) maximize sensitivity to support 2.

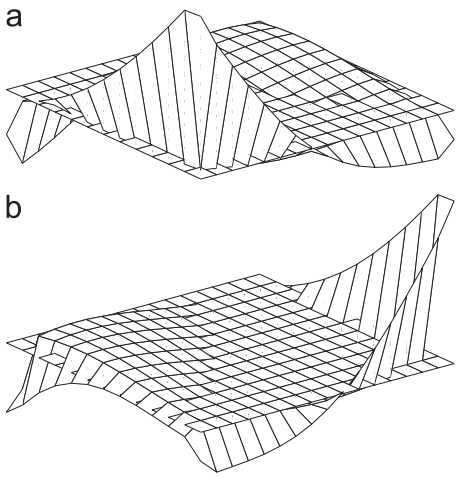

Fig. 12. The distributed sensor shape designed to be sensitive to the support stiffnesses at 40 Hz for the plate example, obtained by maximizing the sensor response: (a) maximize sensitivity to support 1 and (b) maximize sensitivity to support 2.

$S_2/S_4 = 2.3 \times 10^9$. Notice that the shape is very close to that obtained for the first support stiffness and this means that the sensor would have to be manufactured very accurately.

The alternative is to maximize the sensor response. Thus for parameter 1 the sensor shape is given by the eigenvector corresponding to the largest eigenvalue of $\mathbf{T}^{\top}\mathbf{G}_1\mathbf{T}$. Note that this matrix has rank 2. Fig. 12 gives the sensor shapes that are sensitive to parameters 1 and 2, and insensitive to the other parameters. Note that the shapes are now significantly different in the two cases, and that now the thickness change is not very smooth. There are various alternatives that could be considered to produce a sensor shape that is a compromise between those in Figs. 11 and 12.

6. Conclusions

This paper has designed distributed sensors by varying the width (for beams) or thickness (for plates) for structural health monitoring applications. The finite element shape functions are used to define the width or thickness of the sensor and this allows much more flexibility in designing sensors that cover only part of the structure, and other constraints, such as the minimum curvature, may be easily included. It has been demonstrated that sensors may be designed that are sensitive to changes in a single parameter, and insensitive to changes in other parameters. Although much more analysis of these designs is required, the approach does allow the prospect of a simple distributed sensor to monitor a single region, such as a joint, and be insensitive to other changes, such as those arising from environmental changes. The output from such a sensor could have a threshold alarm system, allowing a robust but simple distributed structural health monitoring system. There is significant work still to do before such a method could be applied robustly, including the design of the frequency weighting and the experimental validation of the approach. However the authors hope that this paper will motivate further research to investigate the possibilities.

Acknowledgment

SA gratefully acknowledges the support of the Engineering and Physical Sciences Research Council through the award of an Advanced Research Fellowship.

References

[1] C.-K. Lee, F.C. Moon, Modal sensors/actuators, Journal of Applied Mechanics 57 (1990) 434–441. doi: 10.1115/1.2892008.
[2] R.L. Clark, S.E. Burke, Practical limitations in achieving shaped modal sensors with induced strain materials, Journal of Vibration and Acoustics 118 (1996) 668–675. doi: 10.1115/1.2888350.
[3] M.I. Friswell, Partial and segmented modal sensors for beam structures, Journal of Vibration and Control 5 (1999) 619–637. doi: 10.1177/107754639900500407.
[4] M.I. Friswell, On the design of modal actuators and sensors, Journal of Sound and Vibration 241 (2001) 361–372. doi: 10.1006/jsvi.2000.3300.
[5] D.C. Sun, L.Y. Tong, D.J. Wang, Modal actuator/sensor by modulating thickness of piezoelectric layers for smart plates, AIAA Journal 40 (8) (2002) 1676–1679. doi: 10.2514/2.1840.
[6] J. Kim, J.-S. Hwang, S.J. Kim, Design of modal transducers by optimizing spatial distribution of discrete gain weights, AIAA Journal 39 (10) (2001) 1969–1976.
[7] J. Kim, J.-K. Ryou, S.J. Kim, Optimal gain distribution for two-dimensional modal transducer and its implementation using multi-layered PVDF films, Journal of Sound and Vibration 251 (3) (2002) 395–408. doi: 10.1066/jsvi.2001.4001.
[8] A. Preumont, A. Francois, P. De Man, V. Piefort, Spatial filters in structural control, Journal of Sound and Vibration 265 (1) (2003) 61–79. doi: 10.1016/S0022-460X(02)01440-2.
[9] K.L. Jian, M.I. Friswell, Designing distributed modal sensors for plate structures using finite element analysis, Mechanical Systems and Signal Processing 20 (2006) 2290–2304. doi: 10.1016/j.ymssp.2005.05.010.
[10] K.L. Jian, M.I. Friswell, Distributed modal sensors for rectangular plate structures, Journal of Intelligent Material Systems and Structures 18 (9) (2007) 939–948. doi: 10.1177/1045389X06070589.
[11] N. Tanaka, T. Sanada, Modal control of a rectangular plate using smart sensors and smart actuators, Smart Materials and Structures 16 (1) (2007) 36–46. doi: 10.1088/0964-1726/16/1/004.
[12] A. Donoso, J.C. Bellido, Systematic design of distributed piezoelectric modal sensors/actuators for rectangular plates by optimizing the polarization profile, Structural and Multidisciplinary Optimization 38 (4) (2009) 347–356. doi: 10.1007/s00158-008-0279-7.
[13] A. Donoso, J.C. Bellido, Tailoring distributed modal sensors for in-plane modal filtering, Smart Materials and Structures 18 (3) (2009) 037002, doi: 10.1088/0964-1726/18/3/037002.
[14] A. Donoso, J.C. Carlos Bellido, Distributed piezoelectric modal sensors for circular plates, Journal of Sound and Vibration 319 (1–2) (2009) 50–57. doi: 10.1016/j.jsv.2008.05.033.
[15] S.W. Doebling, C.R. Farrar, M.B. Prime, A summary review of vibration-based damage identification methods, Shock and Vibration Digest 30 (1998) 91–105.
[16] P. Cawley, R.D. Adams, The locations of defects in structures from measurements of natural frequencies, Journal of Strain Analysis 14 (2) (1979) 49–57.
[17] M.I. Friswell, J.E.T. Penny, D.A.L. Wilson, Using vibration data and statistical measures to locate damage in structures, Modal Analysis: The International Journal of Analytical and Experimental Modal Analysis 9 (4) (1994) 239–254.
[18] S.W. Doebling, L.D. Peterson, K.F. Alvin, Estimation of reciprocal residual flexibility from experimental modal data, AIAA Journal 34 (8) (1996) 1678–1685.
[19] M.I. Friswell, J.E.T. Penny, Crack modelling for structural health monitoring, Structural Health Monitoring: An International Journal 1 (2) (2002) 139–148. doi: 10.1177/1475921702001002002.
[20] M.I. Friswell, Damage identification using inverse methods, Royal Society of Philosophical Transactions 365 (2007) 393–410. doi: 10.1098/rsta.2006.1930.
[21] H. Sohn, K. Worden, C.R. Farrar, Statistical damage classification under changing environmental and operational conditions, Journal of Intelligent Material Systems and Structures 13 (9) (2002) 561–574. doi: 10.1106/104538902030904.

[22] D.J. Dawe, Matrix and Finite Element Displacement Analysis of Structures, Oxford University Press, Oxford, 1984.
[23] G. Park, H.H. Cudney, D.J. Inman, An integrated health monitoring technique using structural impedance sensors, Journal of Intelligent Material Systems and Structures 11 (6) (2000) 448–455.
[24] W. Gawronski, J.T. Sawicki, Structural damage detection using modal norms, Journal of Sound and Vibration 229 (1) (2000) 194–198. doi: 10.1006/jsvi.1999.2179.
[25] A. Deraemaeker, A. Preumont, Vibration based damage detection using large array sensors and spatial filters, Mechanical Systems and Signal Processing 20 (7) (2006) 1615–1630. doi: 10.1016/j.ymssp.2005.02.010.
[26] A. Deraemaeker, E. Reynders, G. De Roeck, J. Kullaa, Vibration-based structural health monitoring using output-only measurements under changing environment, Mechanical Systems and Signal Processing 22 (1) (2008) 34–56. doi: 10.1016/j.ymssp.2007.07.004.
[27] C.C. Pagani, Jr., M.A. Trindade, Optimization of modal filters based on arrays of piezoelectric sensors, Smart Materials and Structures 18 (9) (2009) 095046, doi:10.1088/0964-1726/18/9/095046.
[28] B.W. Drinkwater, P.D. Wilcox, Ultrasonic arrays for non-destructive evaluation: a review, NDT & E International 39 (7) (2006) 525–541. doi: 10.1016/j.ndteint.2006.03.006.
[29] P.D. Wilcox, Omni-directional guided wave transducer arrays for the rapid inspection of large areas of plate structures, IEEE Transactions on Ultrasonics Ferroelectrics and Frequency Control 50 (6) (2003) 699–709. doi: 10.1109/TUFFC.2003.1209557.
[30] Y. Ben-Haim, Adaptive diagnosis of faults in elastic structures by static displacement measurement: the method of selective sensitivity, Mechanical Systems and Signal Processing 6 (1) (1992) 85–96. doi: 10.1016/0888-3270(92)90058-Q.
[31] S. Cogan, G. Lallement, Y. Ben-Haim, Updating linear elastic models with modal-based selective sensitivity, in: Proceedings of 12th International Modal Analysis Conference, 1994, pp. 515–520.
[32] Y. Ben-Haim, U. Prells, Selective sensitivity in the frequency domain—I. Theory, Mechanical Systems and Signal Processing 7 (5) (1993) 461–475. doi: 10.1006/mssp.1993.1027.
[33] U. Prells, Y. Ben-Haim, Selective sensitivity in the frequency domain—II. Applications, Mechanical Systems and Signal Processing 7 (6) (1993) 551–574. doi: 10.1006/mssp.1993.1032.
[34] W. Gawronski, Modal actuators and sensors, Journal of Sound and Vibration 229 (4) (2000) 1013–1022. doi: 10.1006/jsvi.1999.2499.